Soft Matter

PAPER

View Article Online
View Journal | View Issue

Cite this: *Soft Matter*, 2021, **17**, 2840

Shape-driven entropic self-assembly of an open, reconfigurable, binary host–guest colloidal crystal†

Timothy C. Moore, [a] Joshua A. Anderson[a] and Sharon C. Glotzer *[ab]

Received 20th November 2020,
Accepted 28th January 2021

DOI: 10.1039/d0sm02073g

rsc.li/soft-matter-journal

Entropically driven self-assembly of hard anisotropic particles, where particle shape gives rise to emergent valencies, provides a useful perspective for the design of nanoparticle and colloidal systems. Hard particles self-assemble into a rich variety of crystal structures, ranging in complexity from simple close-packed structures to structures with 432 particles in the unit cell. Entropic crystallization of open structures, however, is missing from this landscape. Here, we report the self-assembly of a two-dimensional binary mixture of hard particles into an open host–guest structure, where nonconvex, triangular host particles form a honeycomb lattice that encapsulates smaller guest particles. Notably, this open structure forms in the absence of enthalpic interactions by effectively splitting the structure into low- and high-entropy sublattices. This is the first such structure to be reported in a two-dimensional athermal system. We discuss the observed compartmentalization of entropy in this system, and show that the effect of the size of the guest particle on the stability of the structure gives rise to a reentrant phase behavior. This reentrance suggests the possibility for a reconfigurable colloidal material, and we provide a proof-of-concept by showing the assembly behavior while changing the size of the guest particles *in situ*. Our findings provide a strategy for designing open colloidal crystals, as well as binary systems that exhibit co-crystallization, which have been elusive thus far.

1 Introduction

The self-assembly of hard particles has revealed a rich landscape of structures whose assembly and thermodynamic stability are, by virtue of the volume exclusion interactions between particles, driven by entropy.[1] This landscape includes crystalline phases,[2–7] rotator crystal phases,[3,4,6] liquid crystal phases,[4] and quasicrystals.[8,9] Recent work has reported on the self-assembly of hard truncated tetrahedra into a clathrate structure with an astonishing 432 particles in the unit cell.[10]

Recent theoretical work has produced a framework that explains the entropic driving forces of self-assembly in hard particle systems.[11,12] Within this framework, shape entropy gives rise to directional entropic forces (DEFs) that favor facet-aligned, locally dense packings of particles. Hence, structures self-assembled from hard particle building blocks lack porous microstructure, *i.e.*, they are "closed" and not "open" structures.

While shape entropy generally drives the formation of closed structures, open structures are of both theoretical and practical interest.[13] From a theoretical standpoint, it is interesting how different entropic effects can stabilize an open crystalline structure, and how they may drive self-assembly. Practical applications of open structures include photonic materials,[14–16] materials with unique mechanical properties,[17–19] and materials that leverage the porosity, for example, for filtration.[20,21] Shape-driven self-assembly of an open structure would aid in these pursuits by making the self-assembly more robust in practice; an inherent, shape-based drive towards an open structure would allow the addition of specific, synergistic enthalpic interactions to the particles to tune the assembly behavior. Hence, understanding how to design building blocks that favor open structures is of broad interest.

Nonconvex particles offer a promising route to open structures, even within the framework of directional entropic forces, since locally dense packings of concave particles allow the possibility to form porous structures. Despite this possibility, few open/porous structures have been predicted or observed to self-assemble in hard particle systems, and a small but growing body of work has focused on nonconvex particles. Experimental

[a] *Department of Chemical Engineering, University of Michigan, Ann Arbor, MI, USA. E-mail: sglotzer@umich.edu*
[b] *Biointerfaces Institute, University of Michigan, Ann Arbor, MI, USA*

† Electronic supplementary information (ESI) available: Animation showing a single, occupied pore; an animation of the self-assembly; and an animation of one of the reconfigurability simulations. See DOI: 10.1039/d0sm02073g

studies of colloidal hard crosses reveal the self-assembly of chiral rhombic and square 2D crystals,[22] which, despite consisting of concave particles, is still a densest packing arrangement. Simulation studies report the self-assembly of hard, colloidal nanorings into porous smectic structures,[23] the assembly of bowl-shaped particles into worm-like liquids and columnar phases,[24] and the liquid crystalline phase behavior of helical particles.[25–27] Numerical studies on the packing of nonconvex objects have yielded putative densest packings of a wide variety of shapes, ranging from relatively simple crescents and curved triangles[28] to more exotic shapes including the great stellated dodecahedron, a hammerhead shark, and the Stanford Bunny.[29] While the literature on nonconvex hard particles is still growing, it has yet to report self-assembled open structures with long-ranged translational and orientational order.

Multicomponent systems offer another route to form open structures, as the extra component(s) can induce effective entropic attractions between particles that differ from the single-component case, and therefore may stabilize the open structure. However, very few studies have focused on binary, hard particle systems, and none have reported results on multicomponent mixtures containing hard nonconvex particles. Several papers have reported on the phase behavior[30] and design rules for self-assembling binary hard particle mixtures.[5,31,32] Yet, to date, the only studies involving binary systems of anisotropic hard particles that showed self-assembly of substitutionally ordered crystalline structures are a system comprising a space-filling mixture of tetrahedra and octahedra[33] and a mixture of shape allophiles that hierarchically self-assembled a space-filling square lattice.[34] As expected for convex polyhedra within the DEFs framework, the structures in the tetrahedron–octahedron phase diagram are all closed.

Consideration of these possibilities raises the question: can porous structures with long-range order self-assemble in athermal systems, where entropy is the sole driving force? If so, another challenge remains: what kinds of particles in the essentially infinite design space of particle shape should we expect to self-assemble open structures? In this paper, we answer the first question in the affirmative by showing the entropy-driven self-assembly of a binary host–guest structure, where the host particles are located on the sites of an open honeycomb lattice. While entropy has been shown to stabilize an open structure in systems with enthalpic interactions between particles,[35–37] they have not been observed in athermal systems; thus, our results illustrate a novel means of using shape to stabilize a porous, ordered structure. Our results also provide an answer to the second question by showing that a combination of unique concave "host" particles and smaller, convex "guest" particles self-assemble into a host–guest structure with long-range order.

2 Model and methods

We performed two-dimensional Monte Carlo simulations of hard anisotropic particles using the hard particle Monte Carlo (HPMC) module[38] of HOOMD-Blue.[39] We simulated systems comprised of two types of perfectly hard particles (*i.e.*, two different shapes), denoted "host" (H) and "guest" (G) particles, illustrated in Fig. 1. The host particles are regular triangles with edges of length σ, with a thin notch cut out of each edge, rendering them nonconvex. These particles are characterized by the depth d and length l of the notches. We only focus on particles with $l = 0.4$ for the following reasons. For the "uncut" part of each edge to fit into the notch for self-assembly to occur, we have the constraint that $l > 0.33$. The maximum depth of the notch is then defined by the length of the notch; if a notch is too deep, the particle is no longer a single, solid object. Hence, we restrict our focus to a single notch length, one that is long enough to enable the self-assembly, but not so long that the range of possible notch depths is greatly affected. The guest particles are convex polygons, generated by applying an (an)isotropic scaling transformation to regular polygons to modify the aspect ratio and size relative to the host particles. We characterize the size of the guest particles by their aspect ratio and the area they occupy relative to the concave host particles, and denote this ratio s/σ^2. In all HPMC simulations, the sizes of the trial displacements and rotations of the particles were tuned independently to achieve an acceptance rate of 33%. All simulations were performed in an isobaric ensemble. We also included moves on the box aspect ratio and shear. On each MC sweep, we attempted a move on either the box volume, shear, or aspect ratio. In addition to trial moves on the box volume, we attempted moves on the box aspect ratio and shear at each step; all box moves were tuned to achieve a 33% acceptance ratio.

We initialized the systems for self-assembly (both for constant guest size and variable guest size) in a dilute, well-mixed configuration of the particles. The constant guest size self-assembly simulations contained 2400 particles, while the variable guest size simulations contained 900 particles. We then compressed the systems to packing fraction $\phi = 50\%$ and started isobaric simulations. We ran the constant guest size systems for a minimum of 40 million HPMC steps, after which we stopped them if no open hexamer motifs were detected (see below), or continued them until the number of hexamers remained approximately constant for 10 million HPMC steps. We ran the variable

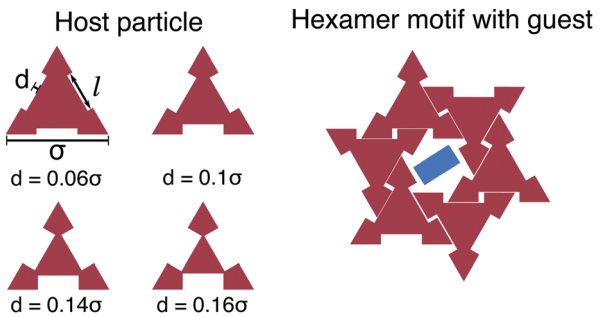

Fig. 1 The particles studied in this work. The host particle is an equilateral triangle with notches cut out of the edges, characterized by the depth d and length l of the notch. The guest particle is a rectangle, characterized by its aspect ratio and area relative to that of the hosts. The guest particle shown here has an aspect ratio of 1:2, and occupies 25% of the area of the host particles in the hexamer motif.

guest size systems for 200 millions HPMC steps. We ran three replicas at each state point for both types of simulations.

The equations of state (EOS) were calculated by decompressing the systems from the ideal solid structure. We first initialized 2400 particles in the crystal structure at the ideal stoichiometry and a packing fraction of 70%, and then performed isobaric simulations at the set pressure. After determining the density had stabilized for at least two million HPMC timesteps, we averaged the packing fraction over the final one million HPMC timesteps. We estimated the statistical error in the packing fraction by averaging over five replicas at each pressure and taking the standard deviation of the mean packing fraction for each system. The EOS curves show two branches connected by a transition region, characteristic of first-order phase transitions commonly observed in hard particle systems. We took the melting pressure to be the average of the two pressures between which the packing fraction showed the largest change.

We define the fraction of the host particles that are part of an open hexamer motif as an order parameter χ, and we define six host particles to constitute an open hexamer motif if they meet the following three criteria. First, to find groups of six particles upon which to test the criteria, we build a neighbor list containing the nearest 14 host particles to each host particle in the system. From this neighbor list, we loop over all groups of six particles. The first criterion is that the six particles must be arranged such that the set of six vectors from the center of the cluster to the centroid of each particle has high hexatic order. This criterion is stated quantitatively as

$$|\psi| = \frac{1}{6}\left|\sum_{j=1}^{6} e^{6i\theta_j}\right| \geq \delta_\psi,$$

where θ_j is the angle between an arbitrary reference vector and the vector from the cluster center to the centroid of the jth particle in the cluster. We used a value of $\delta_\psi = 0.95$ for all analyses. Second, the orientation of each particle in the cluster must be such that the (symmetry-reduced) angle θ_{or} between the vector connecting the center of the cluster to the particle and the vector defining the particle's orientation (*i.e.*, the centroid-to-vertex vector) is close to $\pi/6$. Specifically, we require that θ_{or} be within $\pi/12$ of $\pi/6$. The final criterion requires that each of the six particles in the cluster be within 0.1σ of the mean particle-centroid-to-cluster-center distance. Visual inspection of the systems confirmed that these criteria select the open hexamers, while rejecting similar arrangements of six host particles. Hence, χ is defined as $\chi = N_{H,hex}/N_H$, where $N_{H,hex}$ is the number of host particles in the system that are a part of at least one hexamer that meets the three criteria listed above, and N_H is the total number of host particles in the system.

The computational workflow and data management for this publication were supported by the signac data management framework.[40,41] We utilized the freud analysis library[42] for data analysis and OVITO[43] for system visualization. All plots in this paper were generated with Matplotlib.[44] This work utilizes significant computational resources on XSEDE[45] Stampede2.

3 Results

3.1 Self-assembly of a host–guest structure

A phase diagram from self-assembly simulations in the pressure-stoichiometry plane is shown in Fig. 2a, where we observed several phases to assemble. The systems remained fluid at low pressures and high guest fractions. In contrast, at high pressures and low guest fractions, the systems readily jammed into disordered configurations. Between these two regions, we observed the entropy-driven self-assembly of a unique host–guest structure.

At moderate pressures and fractions of guest particles, the particles self-assembled into an interesting structure with long-range order, as illustrated in Fig. 2c and in the ESI.† The structure consists of the host particles arranged on the sites of a honeycomb lattice, oriented such that the host particles interlock with each other at the notch. This configuration of host particles yields open hexamer motifs of the host particles with roughly hexagonal pores that are occupied by the guest particles. Given this configuration, with the hosts forming pores that the guests occupy, the host particles have well-defined positions and orientations in the lattice, while the guest particles do not, as shown in the ESI.† The unit cell of the structure thus consists of three particles: two interlocking host particles with an orientational offset of $\pi/3$, and the associated guest particle, yielding a stoichiometry of H_2G. We note that the host–guest structure occupies approximately 65–70% of space (*e.g.*, see Fig. 3); however, when considering only the host particles, the packing fraction is much lower, around 30–35%. This network arrangement of the anisotropic host particles yields a chiral structure, where a hexamer of host particles can adopt one of two chiralities, reminiscent of the chiral phase observed in hard equilateral triangles near close-packing.[46] For any given single system, hexamers of both chiralities are observed, albeit in different grains, as the different chiralities are incompatible with one another.

While we find that the optimal assembly (based on the final value of χ) occurs near the H_2G stoichiometry (*i.e.*, where the mole fraction of guests in the system $x_G = 1/3$) as seen in Fig. 2a, we observe the formation of the open hexamer motif in systems away from this stoichiometry as well. In a large excess of guest particles, isolated clusters of host particles arrange into the open hexamer motif, and we often observe two guest particles in the pore that forms, as seen in Fig. 2h. In a large excess of host particles, we find that the host particles tend to trap the few guest particles in the system, as seen in Fig. 2g. The guest particles appear to be required for the host particle hexamers to form, as the host particles do not form the open hexamers in the absence of guest particles, as shown in Fig. 2f and the $x_{G=0}$ slice of Fig. 2a. Instead, the host particles form a distorted triangular lattice in the absence of guest particles; a grain of this crystal can be seen in the middle section of Fig. 2f. Additionally, there is a dependence on the depth of the notch in the host particles on the ability to assemble the open structure; assembly only occurs for particles with a notch depth in the range $0.08\sigma < d < 0.17\sigma$, as shown in Fig. 2b. We find

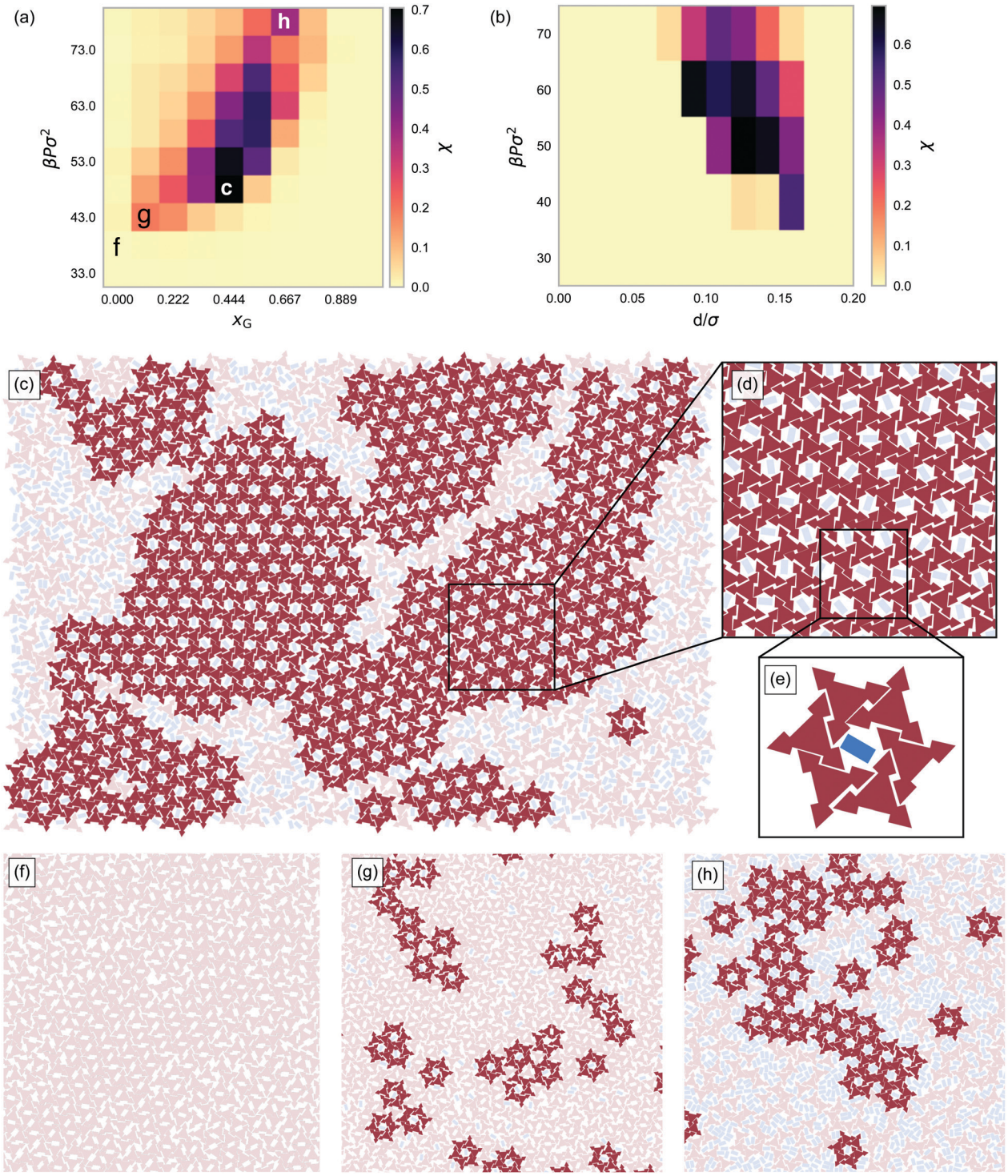

Fig. 2 Self-assembly phase diagrams (a and b) and representative snapshots (c–h) of the binary host–guest systems. The data in (a) was obtained for triangle host particles with a notch depth of 0.1σ, and the data in (b) was obtained at a stoichiometry $x_G = 0.5$. In (a) and (b), the pixel color indicates the value of the order parameter χ (see methods) at the end of the simulations, averaged over 3 replicas (standard deviation of χ across replicas < 0.01). In all snapshots in (c–h), the host particles are characterized by $d = 0.1\sigma$ and $l = 0.4\sigma$. In all cases, the host particles are characterized by a relative size $s/\sigma^2 = 0.25$ and an aspect ratio of 1:2. The snapshot in (c) shows the system with the highest value of the order parameter in (a); the system contains several crystal grains separated by guest-rich fluid regions. Note that the Gibbs phase rule allows up to two phases in thermodynamic equilibrium for a system with a fixed number of particles, pressure, and temperature. Zoomed-in snapshots of a solid region and hexamer motif are shown in (d and e), respectively, showing the details of the host–guest structure. (f–h) show representative motifs from systems in the regions of the phase diagram in (a) denoted by each letter. The guestless system (f) shows several grains of the distorted triangular lattice formed by the host particles. The host-rich system (g) shows sparse, guest-occupied pores surrounded by disordered arrangements of the hosts, and the guest-rich system (h) shows clusters of doubly-occupied pores surrounded by a mixed fluid of host and guest particles. In all snapshots, host particles identified as belonging to a hexamer are highlighted to aid in identifying regions containing the host–guest structure.

that below a notch depth of approximately 0.08σ, no open hexamer motifs are found in the systems, as a result of the effectively smoother edges that allow more entropically-favored edge–edge alignment. Above a notch depth of approximately 0.17σ, we find the systems tend to jam into kinetically arrested configurations, limiting the ability of the systems to form large grains of the host–guest structure. These observations suggest a strong local driving force for the formation of the hexamers of host particles present in the open structure (given the notch depth is within the assembling range), as opposed to the denser local structures that the host particles adopt in the absence of guest particles (as shown in Fig. 2f). These hexamers are compatible with long-range order, and hence these systems form extended host–guest networks under the right conditions. With a picture of the phase diagram, we turn our attention to examining the entropic interactions that stabilize this unique open structure.

3.2 Entropic contributions to stability of host–guest structure

Here, we investigate the question of how entropy is maximized by the host–guest structure. All results we present are from simulations of an isobaric ensemble, and hence the Gibbs free energy $G = -TS + PV$ is the quantity that is minimized (note the PV term in addition to the entropic term). We obtain similar results when sampling an isochoric ensemble, and hence the entropy is the major driving force for the observed behavior. At the finite pressures investigated, the PV term in the free energy is negligible, as we find a negligible volume non-additivity between the host and guest particles. The ideal mixing entropy, proportional to $\sum_{i\in\{H,G\}} x_i \ln x_i$, favors mixing of fluids of the individual species, but does not favor either fluid or crystalline mixed phases. Therefore, the configurational entropy of systems in the crystalline state must be greater than that of systems in fluid states for self-assembly to occur. In the following, we consider the entropies of subsystems composed of host and guest particles separately, and demonstrate that the total system entropy is maximized by sacrificing the entropy of the former for that of the latter. Further, we explain trends that we observe in the context of an entropic attraction between host particles brought about by the presence of the guest particles.

We first consider the relevant contributions to the entropy of the solid host–guest structure. The guests have only weakly defined positions and orientations (*e.g.*, they behave like hard polygons in a discrete plastic crystal mesophase[47]), and therefore have high configurational entropy. In contrast, the hosts have both well-defined positions and orientations, and oscillate about their lattice sites. On a per particle basis, the guest subsystem therefore has a larger entropy than the host subsystem, as the guests are able to explore more of their positional and orientational phase space. Notice also that there is an inherent competition between these two entropies; if the hosts oscillate with a larger amplitude, the average size of the pores decreases, leaving less space available for the guest particles to sample.

Given the athermal nature of these systems, attractions between particles are an entropic effect,[11,12] but we can interpret the melting pressure as a proxy for an effective cohesive free energy between the particles. In the same way that solids with a higher cohesive free energy have higher melting temperatures, structures in athermal hard particle systems with a higher effective cohesive free energy will have lower melting pressures; that is, less external pressure is required to keep the particles in the solid structure. We observe this behavior in the equations of state for these systems, shown as a function of the size and aspect ratio of the guest particles in Fig. 3a–d. In the equations of state, for a given guest particle size, starting from a high pressure and moving to lower pressures, there is a clear melting transition where the density of the system abruptly drops, indicating a first order phase transition. From these equations of state, we determined the melting pressure curves as a function of the size of the guest particles. These melting pressure curves are shown in Fig. 3e.

Fig. 3e shows that for small guest particles, the melting pressure decreases with increasing guest size, indicating an increasing effective cohesive free energy with guest size. This trend is a result of the aforementioned entropic competition in these systems; as the size of the guest particles is increased, the space they can explore is reduced (for a fixed pore size), giving rise to an effective entropic pressure within the pore. To alleviate this pressure, the host particles can increase the size of the pores by packing tighter and oscillating with a smaller amplitude (which costs a small entropic penalty that must be offset by the corresponding gain in configurational entropy of the guest particles). Hence, increasing the size of the guest particles in the host–guest structure leads to an increased effective attraction between the host particles, whose origin is in maximizing the entropy available to the guest particles. This mechanism is similar to the osmotic pressure that depletant molecules exert on colloidal particles in the Asakura–Oosawa model.[48,49] However, in contrast to the usual entropically-driven close packing of colloidal particles seen in depletant systems, the entropic attraction described here drives particles to a lower-density packing as a result of the shape of the host particles.

Clearly, the guest particles will eventually be too large to freely rotate within the pores, even when the pores are as large as possible (dictated by the size of the notches on the host particles). At this point, since the pores cannot become any larger, the maximum effective cohesive free energy between the hosts has been achieved. Therefore, increasing the size of the guest particles at this point only increases the entropic penalty of hindered rotation, and therefore more pressure must be applied to the system to balance the effective entropic pressure within the pores. Here, the magnitude of the slope of the melting pressure curve decreases and eventually the curve inverts, consistent with a decreasing cohesive free energy and stronger driving force for melting with increasing size of the guest particles. To support this picture, Fig. 3e shows the melting pressure curves plotted as a function of the circumsphere radius r_c of the guest particles, and therefore compares systems with square and rectangular guest particles with roughly equal effective sizes. This figure shows that the melting

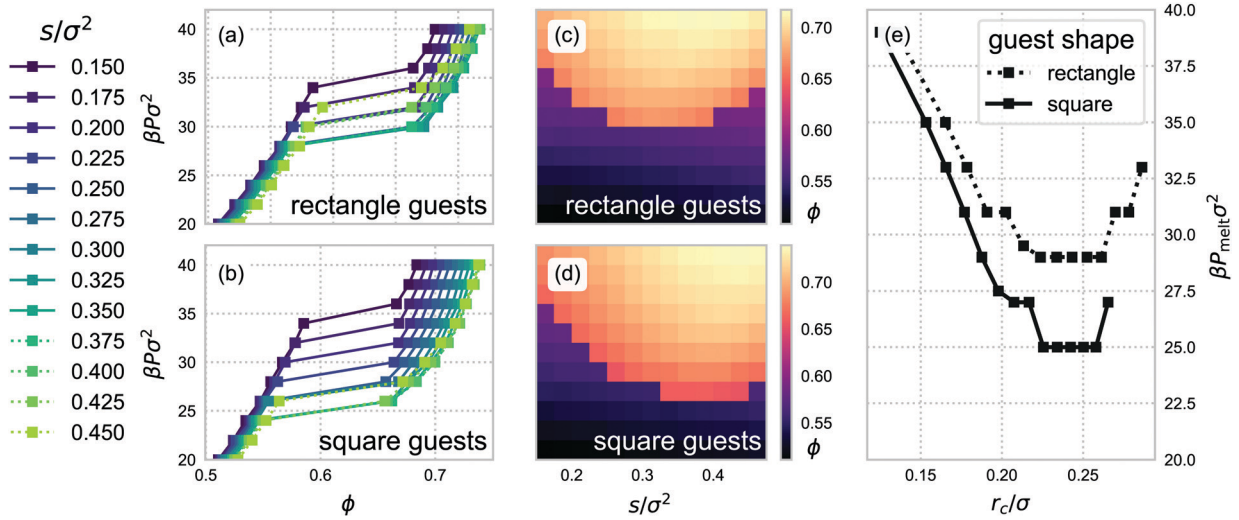

Fig. 3 Equations of state (a–d) and melting pressures (e) for host–guest systems as a function of the size and aspect ratio of the guest particles. The packing fraction ϕ denotes the steady state packing fraction from constant pressure simulations starting from the idealized structure with the ideal stoichiometry x_G = 1/3 and 2400 total particles. The melting pressures were determined as the average of the pressures where the equation of state showed the largest change. For the equations of state, the guest size s/σ^2 is the area that a single guest particle occupies relative to that of a single host particle. The melting pressures are plotted as a function of the circumsphere radius of the guest particle r_c to emphasize the alignment between the two curves when plotted as a function of the effective size of the guest particles. Error bars, estimated as the standard deviation in the melting pressure from 5 independent replicas of each system, are smaller than the symbols. The rectangular guests have an aspect ratio of 2:1, and the hosts are characterized by a notch size of d = 0.1σ, l = 0.4σ.

pressure inversion occurs at approximately the same effective size for both squares and rectangles, although the squares melt at lower pressures than the rectangles. The melting pressure difference between squares and rectangles can be attributed to the symmetry-based increase in orientational entropy of squares compared to rectangles. To see this difference, consider the free energy of an ideal (Einstein) solid, given by[9] $A_{Ein}/NkT = A_{Ein}^{trans} + A_{Ein}^{rot} + A_{Ein}^{mom} - \ln N_{sym}$, where the first two terms are the configurational contributions from translations and rotations, the third term is the momentum contribution from translational motion, and the last term accounts for the symmetry of the particles, where N_{sym} is twice the order of the rotation group of the particle. The first three terms are equal for squares and rectangles, so the difference lies in the symmetry term. Since squares have twice as many symmetries as rectangles, the free energy difference between a crystal of squares compared to rectangles is given by $\Delta A/NkT = A_{rectangles}/NkT - A_{squares}/NkT = \ln(N_{sym}^{squares}/N_{sym}^{rectangles}) = \ln 2 \approx 0.69$. Hence, crystals with rectangular guests have a larger free energy than crystals with square guests, which results in the melting pressure differences observed in Fig. 3. The inversion in the melting pressure curves gives rise to a reentrant phase behavior with respect to the guest particle size, which can be seen clearly in Fig. 3 and is discussed in the next section.

3.3 Leveraging reentrant behavior for reconfigurability

As illustrated in Fig. 3, the nonmonotonic melting pressure as a function of guest particle size indicates reentrant phase behavior. This behavior allows the possibility for a reconfigurable material, where an external stimulus could be used to stimulate a responsive guest particle to change its size and thereby modulate the structure in the system.

As a proof of concept of the reconfigurability allowed by the reentrant phase behavior, we initialize a mixture of host and guest particles at a stoichiometry of x_G = 0.4 and perform HPMC simulations at a constant pressure of $\beta P\sigma^2$ = 40 while changing the size of the guest particles relative to that of the host particles; an animation of this simulation is available in the ESI.† We begin with a relative size ratio of 0.05, and linearly increase to 0.6 over the course of 100 million MC steps; the guest particles are then returned to their original size during the following 100 million MC steps. During the "growth" phase of this procedure, we observe the formation of several clusters of the host–guest structure, as illustrated in Fig. 4c. This assembly is reflected in the order parameter, which initially increases with the size of the guest particle, as shown in Fig. 4a. However, once the guest particles reach a certain size, the host–guest structure is no longer stable and begins to melt, as predicted by the melting pressure trends and as indicated by the decrease in the order parameter beginning around 70 million MC steps. This transition occurs when the relative size of the guest particle is approximately 0.45, which is also the point where the melting pressure curve inverts for square guests (Fig. 3d). By the time the guest particles reach a relative size of 0.6, the hexamers have nearly completely melted and the system is in the well-mixed fluid state depicted in Fig. 4d. Upon shrinking the guest particles from their maximum size, the particles again assemble into clusters of the host–guest structure, which eventually melt once the guest particles shrink below a certain size. Notably, the order parameter *versus* HPMC step curve is roughly symmetric about the point where the guest

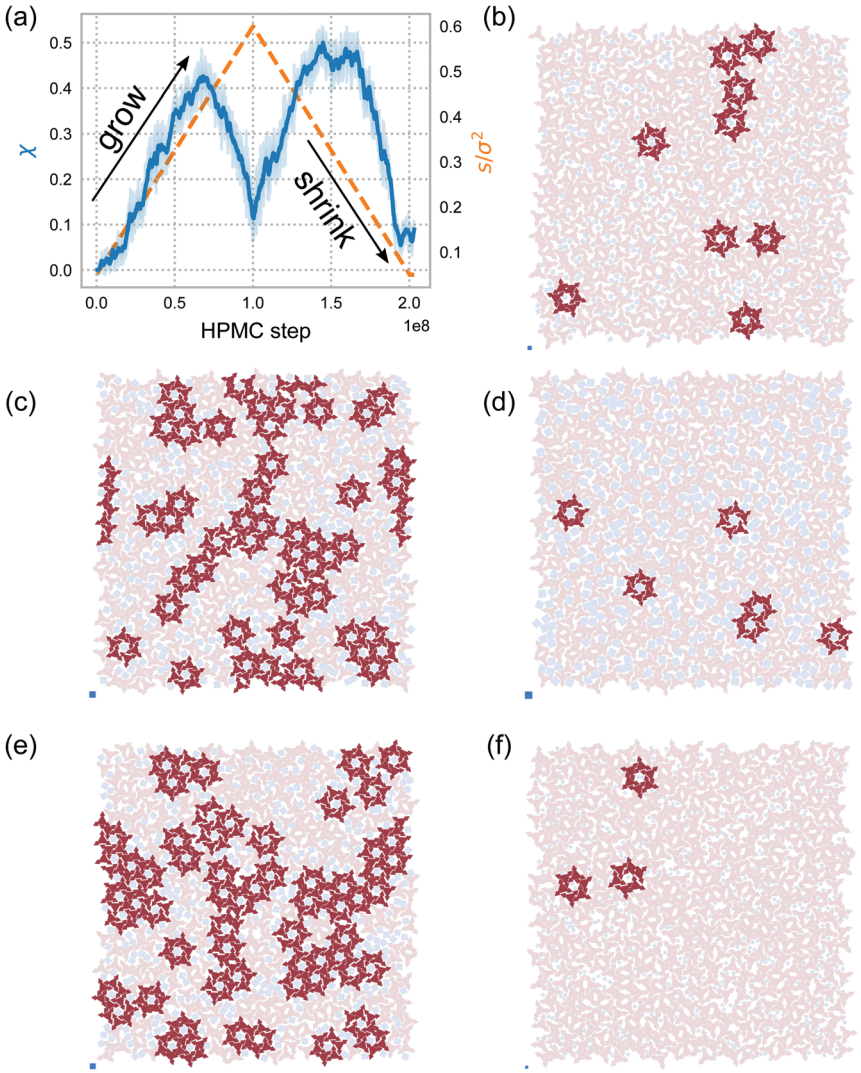

Fig. 4 Reconfigurable host–guest assembly with an *in situ* varying guest particle size. The relative size of the guest particle s/σ^2 is varied throughout the simulation, starting very small, growing, and shrinking back to the original size. (a) The guest size is represented by the dashed orange (lighter) line, and the order parameter χ is depicted by the solid blue (darker) line. The solid line represents the rolling average of the order parameter over a window of 10 simulation snapshots, and the lighter shading represents the instantaneous values. (b–f) Snapshots of the systems during reconfigurability simulations, with the size of the guest particle shown in the lower left of each snapshot. Snapshots taken from the following HPMC steps: (b) 0.2×10^8, (c) 0.7×10^8, (d) 1.0×10^8, (e) 1.4×10^8, and (f) 2.0×10^8. The highlighted host particles in (b–f) are those identified as being a part of the open hexamer motif, as defined in Section 2, and the host and guest particles are drawn to scale. The order parameter χ quantifying the amount of host–guest structure in the system shows that the structure assembles when the guest particle is within a range of specific sizes relative to the host, illustrating the possibility of using this type of system as a reconfigurable material. The host particles in this simulation are characterized by a notch size of $d = 0.1\sigma$ and $l = 0.4\sigma$, the guest particles are characterized by a constant aspect ratio of 1:1, and the stoichiometry is fixed at $x_{G=0.4}$.

particles are at a maximum size, illustrating the equilibrium nature of this reconfigurable transition. One may notice that the value of the order parameter never reaches the maximum value obtained during the constant-guest-size self-assembly simulations; this result stems from the fact that we are changing the guest size on a finite time scale. It is certainly possible to optimize the system parameters to maximize crystallization during reconfigurability; such efforts are the focus of ongoing work.

While this *in situ* structural transition triggered by a change in particle properties is easily performed in simulation, a similar transition can be realized in experimental systems. Recent experimental work studying colloidal particles in a polymer solution containing thermosensitive microgel particles showed material reconfigurability based on the thermoresponsive properties of the particles.[50] Taking it one step further, it is possible to change not only particle size, but particle shape on-the-fly in experiment.[51] Considering the melting pressure differences between systems with square *versus* rectangular guest particles, there is the possibility for a shape-change-induced structural transformation with a shape-changing guest particle. We emphasize that by virtue of the volume–exclusion interactions between particles, the behavior in this system is driven solely by entropy; therefore, we expect the same behavior to be observed in similar experimental systems in conditions where enthalpic interactions have been effectively

removed. This scenario can be realized, *e.g.*, by modifying the solvent and/or environmental conditions.[52,53]

The reconfigurability discussed here is only possible because of the two-component nature of our systems, where the relative sizes of the particles can be varied. In contrast, particle size changes in a single-component system only change the packing fraction. Shape-induced transitions have also been described previously, *e.g.*, between cubic phases in colloidal polyhedra.[54] Here, we have shown that the relative shape and size of particles in a binary mixture can have a large influence on the phase behavior and therefore provide useful variables to act as the controller in a reconfigurable colloidal material.

4 Conclusions

We have demonstrated the self-assembly of an open host–guest structure in a binary, hard anisotropic particle system. The nonconvex nature of the host particles and relative size of the guest particles result in a system where the entropy of a host–guest structure that comprises a porous network of host particles filled with guest particles is greater than that of any disordered phase. This system represents one of the first self-assembled binary structures with long-range order in an athermal system of anisotropic particles.

While particle shape is now well understood to play an important role in determining the crystal structure of nanoparticle superlattices, the current study is the first to show how particle shape alone can be used to target an open structure. While the results presented herein represent a simplified picture of the complex interactions that occur between colloidal particles, they nonetheless offer useful information for the experimentalist. We show that nonconvex triangular particles can form an interlocking, open structure when mixed with a guest that can fit within its pores, and that the effective attraction between the nonconvex particles is driven by an entropic force originating with the guest particles. The notched triangles studied in this work are experimentally accessible, *e.g.*, through nanolithographic techniques.[55] We also note that in this athermal system, the concavity of the particle is essential to the stability of the structure, as it directs the effective attractions between the host particles. We speculate that this effective interaction could be replaced with explicit attractive patches on a convex host particle, a topic for future work.

We showed that the guest particles are necessary for the assembly, and that the size ratio of the host and guest particles is a sensitive parameter for the stability of the structure. We used this sensitivity to highlight the possibility for a reconfigurable system; by controlling the size and/or shape of the guest particles, for example, similar to what has been shown for polymer hydrogel systems,[50] there is the possibility to control the morphology of the system. Such reconfigurability allows this type of material to be used as an actuator in a nanoscale machine.

The fact that there is a shape-induced driving force towards this structure means that its assembly is driven by entropy; therefore, specific, directional enthalpic interactions compatible with the hexamer motif may be added to lower the free energy of the structure even further, and make its assembly more robust. This is in contrast to scenarios where the enthalpically- and entropically-favored products differ, and care must be taken to balance the competition between the two. These results therefore provide a new strategy towards the self-assembly of open colloidal lattices.

Author contributions

TCM designed and performed the simulations and analyzed the data. All authors contributed to the writing of the manuscript. SCG directed the research.

Conflicts of interest

There are no conflicts to declare.

Acknowledgements

This research was supported in part by the National Science Foundation, Division of Materials Research Award No. DMR 1808342 and by a grant from the Simons Foundation (256297, SCG). This work used resources from the Extreme Science and Engineering Discovery Environment (XSEDE), which is supported by National Science Foundation grant number ACI-1548562; XSEDE Award DMR 140129. Computational resources and services were supported by Advanced Research Computing at the University of Michigan, Ann Arbor. The authors would like to acknowledge fruitful discussions with Jens Glaser, Sangmin Lee, and R. Allen LaCour.

References

1 F. Sciortino, *La Rivista del Nuovo Cimento*, 2019, **42**, 511–548.
2 B. J. Alder and T. E. Wainwright, *J. Chem. Phys.*, 1957, **27**, 1208–1209.
3 U. Agarwal and F. A. Escobedo, *Nat. Mater.*, 2011, **10**, 230–235.
4 P. F. Damasceno, M. Engel and S. C. Glotzer, *Science*, 2012, **337**, 453–457.
5 B. A. Schultz, P. F. Damasceno, M. Engel and S. C. Glotzer, *ACS Nano*, 2015, **9**, 2336–2344.
6 D. Klotsa, E. R. Chen, M. Engel and S. C. Glotzer, *Soft Matter*, 2018, **14**, 8692–8697.
7 P. F. Damasceno, M. Engel and S. C. Glotzer, *ACS Nano*, 2012, **6**, 609–614.
8 A. Haji-Akbari, M. Engel, A. S. Keys, X. Zheng, R. G. Petschek, P. Palffy-Muhoray and S. C. Glotzer, *Nature*, 2009, **462**, 773–777.
9 A. Haji-Akbari, M. Engel and S. C. Glotzer, *J. Chem. Phys.*, 2011, **135**, 194101.
10 S. Lee, E. G. Teich, M. Engel and S. C. Glotzer, *Proc. Natl. Acad. Sci. U. S. A.*, 2019, **116**, 14843–14851.
11 G. van Anders, N. K. Ahmed, R. Smith, M. Engel and S. C. Glotzer, *ACS Nano*, 2014, **8**, 931–940.

12 G. van Anders, D. Klotsa, N. K. Ahmed, M. Engel and S. C. Glotzer, *Proc. Natl. Acad. Sci. U. S. A.*, 2014, **111**, E4812–E4821.
13 B.-L. Su, C. Sanchez and X.-Y. Yang, *Hierarchically structured porous materials: from nanoscience to catalysis, separation, optics, energy, and life science*, John Wiley & Sons, 2012.
14 J. F. Galisteo-López, M. Ibisate, R. Sapienza, L. S. Froufe-Pérez, Á. Blanco and C. López, *Adv. Mater.*, 2011, **23**, 30–69.
15 J. D. Joannopoulos, P. R. Villeneuve and S. Fan, *Nature*, 1997, **386**, 143–149.
16 A. Moroz, *Phys. Rev. B: Condens. Matter Mater. Phys.*, 2002, **66**, 115109.
17 G. N. Greaves, A. L. Greer, R. S. Lakes and T. Rouxel, *Nat. Mater.*, 2011, **10**, 823–837.
18 J. N. Grima, R. Gatt, V. Zammit, J. J. Williams, K. E. Evans, A. Alderson and R. I. Walton, *J. Appl. Phys.*, 2007, **101**, 086102.
19 G. Ernst, C. Broholm, G. R. Kowach and A. P. Ramirez, *Nature*, 1998, **396**, 147–149.
20 M. E. Davis and R. F. Lobo, *Chem. Mater.*, 1992, **4**, 756–768.
21 M. E. Davis, *Nature*, 2002, **417**, 813–821.
22 K. Zhao and T. G. Mason, *J. Phys.: Condens. Matter*, 2014, **26**, 152101.
23 C. Avendaño, G. Jackson, E. A. Müller and F. A. Escobedo, *Proc. Natl. Acad. Sci. U. S. A.*, 2016, **113**, 9699–9703.
24 M. Marechal and M. Dijkstra, *Phys. Rev. E: Stat., Nonlinear, Soft Matter Phys.*, 2010, **82**, 031405.
25 H. B. Kolli, E. Frezza, G. Cinacchi, A. Ferrarini, A. Giacometti, T. S. Hudson, C. De Michele and F. Sciortino, *Soft Matter*, 2014, **10**, 8171–8187.
26 S. Dussi and M. Dijkstra, *Nat. Commun.*, 2016, **7**, 1–10.
27 H. B. Kolli, G. Cinacchi, A. Ferrarini and A. Giacometti, *Faraday Discuss.*, 2016, **186**, 171–186.
28 S. Atkinson, Y. Jiao and S. Torquato, *Phys. Rev. E: Stat., Nonlinear, Soft Matter Phys.*, 2012, **86**, 031302.
29 J. de Graaf, R. van Roij and M. Dijkstra, *Phys. Rev. Lett.*, 2011, **107**, 155501.
30 M. R. Khadilkar, U. Agarwal and F. A. Escobedo, *Soft Matter*, 2013, **9**, 11557–11567.
31 M. R. Khadilkar and F. A. Escobedo, *Phys. Rev. Lett.*, 2014, **113**, 165504.
32 F. A. Escobedo, *J. Chem. Phys.*, 2017, **147**, 214501.
33 A. T. Cadotte, J. Dshemuchadse, P. F. Damasceno, R. S. Newman and S. C. Glotzer, *Soft Matter*, 2016, **12**, 7073–7078.
34 E. S. Harper, R. L. Marson, J. A. Anderson, G. van Anders and S. C. Glotzer, *Soft Matter*, 2015, **11**, 7250–7256.
35 X. Mao, Q. Chen and S. Granick, *Nat. Mater.*, 2013, **12**, 217–222.
36 X. Mao, *Phys. Rev. E: Stat., Nonlinear, Soft Matter Phys.*, 2013, **87**, 062319.
37 D. Z. Rocklin and X. Mao, *Soft Matter*, 2014, **10**, 7569–7576.
38 J. A. Anderson, M. E. Irrgang and S. C. Glotzer, *Comput. Phys. Commun.*, 2016, **204**, 21–30.
39 J. A. Anderson, J. Glaser and S. C. Glotzer, *Comput. Mater. Sci.*, 2020, **173**, 109363.
40 C. S. Adorf, P. M. Dodd, V. Ramasubramani and S. C. Glotzer, *Comput. Mater. Sci.*, 2018, **146**, 220–229.
41 C. S. Adorf, V. Ramasubramani, B. D. Dice, M. M. Henry, P. M. Dodd and S. C. Glotzer, *glotzerlab/signac*, 2019, DOI: 10.5281/zenodo.2581327.
42 V. Ramasubramani, B. D. Dice, E. S. Harper, M. P. Spellings, J. A. Anderson and S. C. Glotzer, *Comput. Phys. Commun.*, 2020, 107275.
43 A. Stukowski, *Modell. Simul. Mater. Sci. Eng.*, 2009, **18**, 015012.
44 J. D. Hunter, *Comput. Sci. Eng.*, 2007, **9**, 90–95.
45 J. Towns, T. Cockerill, M. Dahan, I. Foster, K. Gaither, A. Grimshaw, V. Hazlewood, S. Lathrop, D. Lifka, G. D. Peterson, R. Roskies, J. R. Scott and N. Wilkins-Diehr, *Comput. Sci. Eng.*, 2014, **16**, 62–74.
46 A. P. Gantapara, W. Qi and M. Dijkstra, *Soft Matter*, 2015, **11**, 8684–8691.
47 W. Shen, J. Antonaglia, J. A. Anderson, M. Engel, G. van Anders and S. C. Glotzer, *Soft Matter*, 2019, **15**, 2571–2579.
48 S. Asakura and F. Oosawa, *J. Chem. Phys.*, 1954, **22**, 1255–1256.
49 S. Asakura and F. Oosawa, *J. Polym. Sci.*, 1958, **33**, 183–192.
50 L. Rossi, V. Soni, D. J. Ashton, D. J. Pine, A. P. Philipse, P. M. Chaikin, M. Dijkstra, S. Sacanna and W. T. M. Irvine, *Proc. Natl. Acad. Sci. U. S. A.*, 2015, **112**, 5286–5290.
51 K. J. Lee, J. Yoon, S. Rahmani, S. Hwang, S. Bhaskar, S. Mitragotri and J. Lahann, *Proc. Natl. Acad. Sci. U. S. A.*, 2012, **109**, 16057–16062.
52 J. Henzie, M. Grünwald, A. Widmer-Cooper, P. L. Geissler and P. Yang, *Nat. Mater.*, 2012, **11**, 131–137.
53 T. B. Martin and A. Jayaraman, *Mater. Res. Express*, 2016, **3**, 034001.
54 C. X. Du, G. van Anders, R. S. Newman and S. C. Glotzer, *Proc. Natl. Acad. Sci. U. S. A.*, 2017, **114**, E3892–E3899.
55 M. Zhang, V. Pacheco-Peña, Y. Yu, W. Chen, N. J. Greybush, A. Stein, N. Engheta, C. B. Murray and C. R. Kagan, *Nano Lett.*, 2018, **18**, 7389–7394.

